Journal of Hazardous Materials 197 (2011) 19–25

Contents lists available at SciVerse ScienceDirect

Journal of Hazardous Materials

journal homepage: www.elsevier.com/locate/jhazmat

Nanopaper based on Ag/TiO_2 nanobelts heterostructure for continuous-flow photocatalytic treatment of liquid and gas phase pollutants

Weijia Zhou[a], Guojun Du[a], Peiguang Hu[a], Yongquan Yin[b], Jianhua Li[a], Jiahong Yu[b], Guancong Wang[a], Jinxia Wang[c], Hong Liu[a,*], Jiyang Wang[a], Hua Zhang[d]

[a] State Key Laboratory of Crystal Materials, Center of Bio & Micro/Nano Functional Materials, Shandong University, 27 Shandanan Road, Jinan 250100, PR China
[b] The School of Environmental Science and Engineering, Shandong University, 27 Shandanan Road, Jinan 250100, PR China
[c] School of Light Chemistry and Environment Engineering, Shandong Polytechnic University, Daxue Road, Western University Science Park, Jinan 250353, PR China
[d] School of Materials Science and Engineering, Nanyang Technological University, 50 Nanyang Avenue, Singapore 639798, Singapore

ARTICLE INFO

Article history:
Received 13 April 2011
Received in revised form 27 August 2011
Accepted 13 September 2011
Available online 17 September 2011

Keywords:
TiO_2 nanobelts
Heterostructures
Nanopapers
Continuous photocatalysis
Antibacterial property

ABSTRACT

The Ag/TiO_2 nanobelt heterostructures were prepared by the acid-assisted hydrothermal method followed by an in situ photo-reduction process. The photocatalytic activity of TiO_2 nanobelts was evidently enhanced by the heterostructures between Ag nanoparticles and TiO_2 nanobelts. The nanopapers based on Ag/TiO_2 nanobelt heterostructures were fabricated via a modified paper-making process. A novel continuous photocatalytic reactor was designed, and MO removal rate of Ag/C–TiO_2 nanopaper was achieved to 100% in 40 min for single layer and only in 6 min for three layers. The self-supported TiO_2 nanopapers with porous structures also showed an excellent continuous photocatalytic performance for toluene gas under UV light irradiation, and the corresponding degradation rate was 69.5% in 184 min. Moreover, the Ag/TiO_2 nanobelts nanopaper showed a good antibacterial effect. The multifunctional TiO_2 nanopapers modified by the heterostuctures could have potential applications in the environmental and biomaterial fields.

1. Introduction

Titanium dioxide (TiO_2) has been intensively investigated as a semiconductor photocatalyst since Fujishima and Honda discovered the photocatalytic splitting of water on TiO_2 electrodes in 1972 [1]. Many studies have shown the association between environmental quality and health problems. In addition, bacteria and fungi can also be disseminated from contaminated water and air to affect human health. Recently, the application of TiO_2 photocatalysts has mainly been focused on the decomposition of toxic and hazardous organic pollutants in the contaminated water and air, which is of great importance for the environmental protection [2–5]. In particular, a commercial TiO_2 polycrystalline nanopowder, Degussa P-25, a mixture of anatase (80%) and rutile (20%), has exhibited enhanced photocatalytic activity, which is the most widely used photocatalyst in wastewater treatment. However, the separation of nanosized photocatalyst particles from wastewater and their recycling are difficult and uneconomical due to the small particle size. To resolve the problem, various methods, such as immobilization of TiO_2 particles on substrates (optical fibers, silica particles, etc.) have been widely investigated [6–9]. However, the low loaded capacity, the limited surface area and catalyst attrition are main drawbacks.

One-dimensional TiO_2 nanomaterials have properties that compare with TiO_2 nanoparticles but possess a high surface-to-volume ratio, rapid diffusion-free electron transport along the long direction, and the low number of grain boundaries. Kasuga et al. first discovered the alkaline hydrothermal route for synthesis of titanium oxide with a tubular shape, which attracts a great deal of interest [10]. In particular, TiO_2 nanobelts with a large aspect ratio can be separated easily from wastewater, which overcomes the recycling drawbacks. Although the notable advances have been made, the high recombination rate of the photogenerated electron/hole pairs and less active surface sites hinder TiO_2 nanobelts further applications in industry. Numerous studies have suggested that the deposition of Ag nanoparticles (AgNPs) on TiO_2 photocatalyst can highly improve its photocatalytic efficiency through the Schottky barrier conduction band electron trapping and consequent longer electron-hole pair lifetime [11–13].

Based on the above technologies, TiO_2 nanobelts with a high photocatalytic activity in the batch were obtained in the paper. However, it is also an intermittent photocatalytic reaction, and the recovery of the catalyst will increase the costs of equipment and production. So, large scale-fabrication of TiO_2 nanobelts with a

* Corresponding author. Tel.: +86 0531 88362807.
E-mail addresses: hongliu@sdu.edu.cn (H. Liu), jywang@icm.sdu.edu.cn (J. Wang).

0304-3894/$ – see front matter.
doi:10.1016/j.jhazmat.2011.09.051

high catalytic activity into paper-like 2D freestanding membranes and the corresponding continuous-flow photocatalysis are urgent to be solved [14–16]. Herein, we report a method to improve the photocatalytic activity of TiO_2 nanobelts by acid corrosion then loading AgNPs. The TiO_2 paper-like 2D freestanding membranes were fabricated by a modified paper-making process. A highly efficient TiO_2 nanopaper-based continuous-flow microreactor was designed, which was used for continuous photocatalytic treatment of methyl orange aqueous solution and toluene gas pollutants. The antibacterial performance of TiO_2 nanopaper loaded with AgNPs was also tested.

2. Experimental

2.1. Materials

Titania P-25 (TiO_2; ca. 80% anatase and 20% rutile), sodium hydroxide (NaOH), hydrochloric acid (HCl), sulfuric acid (H_2SO_4), and silver nitrate ($AgNO_3$) were purchased from China National Medicines Corporation Ltd. All chemicals were analytical grade without further purification. Deionized water was used throughout this study.

2.2. Preparation of photocatalysts

2.2.1. TiO_2 nanobelts

Titanate nanobelts were synthesized by the hydrothermal process in concentrated NaOH aqueous solution. A commercial Titania P-25 was used as the precursor, and a typical synthesis process is shown as follows: 1 g precursor was mixed with 80 mL of 10 M NaOH aqueous solution, followed by hydrothermal treatment at 180 °C in a 100 mL Teflon-lined autoclave for 48 h. The treated powder was washed thoroughly with deionized water followed by a filtration and drying process. The sodium titanate nanobelts were obtained. These were immersed in 0.1 M HCl aqueous solution for 24 h and then washed thoroughly with water to get $H_2Ti_3O_7$ nanobelts. After the $H_2Ti_3O_7$ nanobelts were isolated from the solution by centrifugation and sequentially washed with deionized water for several times, they were dried at 70 °C for 10 h. Finally, TiO_2 nanobelts were obtained by annealing the $H_2Ti_3O_7$ nanobelts at 600 °C for 2 h.

2.2.2. TiO_2 nanobelts with acid corrosion

After the obtained H-titanate nanobelts were added into a 100 mL Teflon vessel, 0.02 M H_2SO_4 aqueous solution was filled up to 80% of the total volume of the vessel, which was kept at 100 °C for 12 h. Then the products were isolated from the solution by centrifugation and sequentially washed with deionized water for several times, and then dried at 70 °C for 10 h. By annealing the hydrogen titanate obtained by acid corrosion at 600 °C for 2 h, anatase TiO_2 nanobelts with rough surface were obtained, which was expressed as C–TiO_2 nanobelts.

2.2.3. Ag/C–TiO_2 nanobelt heterostructure

Ag/C–TiO_2 nanobelt heterostructures were prepared by the photo-reduction method based on C–TiO_2 nanobelts. Briefly, after 0.5 g $AgNO_3$ was dissolved in 50 mL ethanol solution, 0.5 g TiO_2 nanobelt was added in it. The obtained mixing solution was illuminated with a 20 W ultraviolet lamp for 1 min under magnetic agitation. After illumination, the product was thoroughly washed with distilled water and dried at room temperature, which was expressed as Ag/C–TiO_2 nanobelts.

2.2.4. TiO_2 freestanding nanopapers

TiO_2 nanobelt-based nanopapers were fabricated by a modified paper-making process referred to literatures [14,15]. Briefly, 1 g TiO_2 nanobelts without any surfactants were dispersed in 1L distilled water under magnetic stirring, followed by filtering the resultant pulp on a sub-microporous filter paper (pore size of 0.22 μm) surface through a vacuum-filter (SHB-III, Hi-tech Instrument BritishYu Gongyi City, and the vacuum is 0.1 Mpa) with ceramic filter (pore size of 0.45 μm). TiO_2 nanopapers were fabricated by compacting under 0.1 Mpa pressure and drying the wet TiO_2 sheet at 70 °C for 24 h. The C–TiO_2 and Ag/C–TiO_2 nanopapers were fabricated by the same process.

2.3. Characterization of catalysts

X-ray powder diffraction (XRD) pattern of catalysts were recorded on a Bruke D8 Advance powder X-ray diffractometer with Cu Kα (λ = 0.15406 nm). HITACHI S-4800 field emission scanning electron microscope (FE-SEM) was used to characterize the morphologies and size of the synthesized samples. The chemical composition was investigated via energy-dispersive X-ray spectroscopy (EDX). High resolution transmission electron microscopy (HRTEM) images were carried out with a JOEL JEM 2100 microscope.

2.3.1. Batch and continuous-flow photocatalytic reaction

Methyl orange (MO) was selected as the model chemical to evaluate the activity and properties of the different photocatalysts. In a typical experiment, 20 mL aqueous suspensions of MO (25 mg/L) and 20 mg of photocatalyst powders were placed in a 50 mL beaker. Prior to irradiation, the suspensions were magnetically stirred in the dark for 60 min to establish adsorption/desorption equilibrium between the dye and the surface of the catalyst under room air equilibrated conditions. A 300 W lamp with main emission at 365 nm was used as the UV resource for UV light photocatalysis. At the given irradiation time intervals, the mixed solution were collected and centrifuged to remove the catalyst particulates for analysis. The residual MO concentration was detected using a UV–vis spectrophotometer (Hitachi UV-3100).

The schematic diagram of the continuous photocatalytic microreactor and system was shown in Fig. 1. The device consists of built-in UV lamp (1), quartz tube (2), porous glass funnel (3), anti-UV glass tube (5) and cap (6). UV lamp (1) is vertically placed in the inner quartz tube (2) of the reactor. A power cord (9) exits from the top side of the cover. Quartz tube cap covers on the outside of UV lamp for protection from corrosion of liquid or air pollution, and quartz glass does not block the UV radiation. Porous funnels were installed on the outside of the quartz tube (2), which can be adjusted according to different requirements. The angle between porous funnel wall and the quartz tube is 30 degrees, which makes the catalyst papers fully accept UV irradiation. The session numbers of porous funnel and pore volume and diameter of funnel walls can be changed as required to control the filtration rate. Here, the height of a single funnel is 5 cm, and the volume is 100 cm^3. Porous TiO_2 nanobelt-based filter papers (4) placed on the inner wall of the funnels. The MO aqueous solution (25 mg/L) is pumped with a flow rate of 20 mL/min into the upper inlet (7) of the photocatalytic reactor by a cross-flow pump. UV light radiates through the quartz tube to the TiO_2 nanopapers, and simultaneously MO aqueous solution flows through the TiO_2 nanopapers, leading to the photocatalytic degradation reaction. The degradation produces are discharged from the water outlet (8) of the photocatalytic reactor.

The device can be simply reconstructed for gas continuous-flow photocatalytic reaction with different TiO_2 nanopapers for toluene gas. Prior to irradiation reaction, the toluene gas were cycled through the TiO_2 nanobelts nanopaper in the dark for 60 min to establish adsorption/desorption equilibrium between the gas and the surface of the catalyst under room air equilibrated conditions. The circulation velocity was set to 1 L/min. After that, the

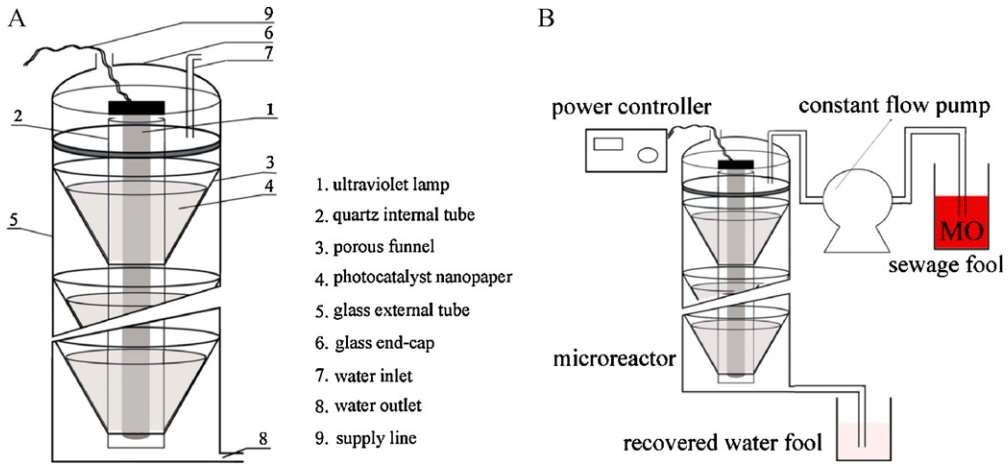

Fig. 1. Experimental set up used in the liquid-phase degradation of methyl orange (MO) solution with a 36 W UV lamp as the UV light resource: (A) photocatalytic microreactor and (B) continuous-flow microreactor.

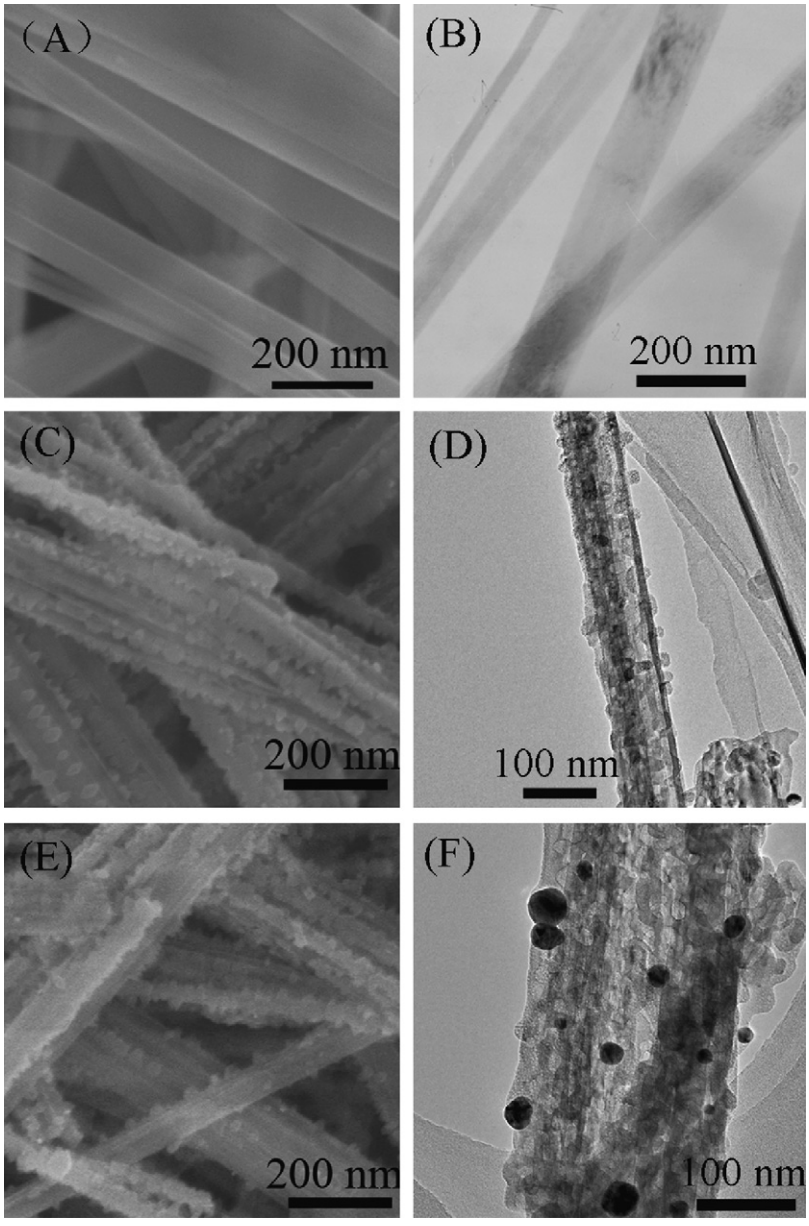

Fig. 2. Typical SEM and TEM images of the as-synthesized (A and B) TiO_2 nanobelts, (C and D) C–TiO_2 nanobelts and (E and F) Ag/C–TiO_2 nanobelts.

Table 1
EDX elemental composition of (a) TiO_2 nanobelts, (b) C–TiO_2 nanobelts and (c) Ag/C–TiO_2 nanobelts.

Samples	Ti		O		Ag	
	wt%	at.%	wt%	at.%	wt%	at.%
a	58.93	32.35	41.07	67.65	–	–
b	56.05	29.83	43.05	70.17	–	–
c	55.83	30.19	42.84	69.49	1.33	0.32

initial concentration of toluene gas in the reactor was tested with the value of about 12 mg/L. A 36 W UV lamp with main emission at 355 nm was used as the UV resource for UV light photocatalysis. At the given irradiation time intervals, the gas in the reactor was collected to analysis the residual concentration of toluene with the characteristic peak area, which was measured by gas chromatography (SP-6800A; Shandong Lunan Ruihong Chemical Instrument Ltd., China).

2.4. Bactericidal test

To examine the bactericidal effect of the different papers, approximately 10^5 colony forming units (CFU) of *E. coli* strain B were cultured on lysogeny broth (LB) agar plates. The conventional filter paper, TiO_2, C–TiO_2 and Ag/C–TiO_2 nanopapers and LB plates were cultured under the same conditions. After the plates were incubated at 37 °C for 24 h, the numbers of colonies were counted.

3. Results and discussion

The typical SEM and TEM images of the as-synthesized TiO_2 nanobelts, C–TiO_2 nanobelts and Ag/C–TiO_2 nanobelts were shown in Fig. 2. Fig. 2A and B shows typical images of the as-prepared TiO_2 nanobelts with width of 50–200 nm, and lengths of up to hundreds of micrometers. Fig. 2C and D are low-magnification SEM and TEM images of the TiO_2 nanobelts treated with acid corrosion, which possesses the porous and rough surface. The one-dimensional morphology of TiO_2 nanobelts was not destroyed by acid corrosion, while more activated surface was obtained. The SEM image of Ag/TiO_2 nanobelts with acid corrosion was shown in Fig. 2E. AgNPs were not clearly observed on the TiO_2 nanobelts due to the rough surface. But the TEM image confirmed the formation of a novel heterostructure between TiO_2 nanobelts and AgPNs due to high phase contrast between them (Fig. 2F). The XPS results of Ag/C–TiO_2 nanobelt also confirmed the existence of the Ag on the TiO_2 nanobelts, which are shown in Fig. S1. Energy dispersive X-ray spectroscopy (EDX) analysis (Table 1) revealed that the TiO_2 nanobelts and C–TiO_2 nanobelts are only composed of Ti and O elements, the atomic ratio of which is about 1:2. Ag/C–TiO_2 nanobelt heterostructures are composed of Ti, O and Ag elements, which were further revealed by EDX and the weight percent of Ag is about 1.33 wt%.

XRD patterns of TiO_2 nanobelts, C–TiO_2 nanobelts and Ag/C–TiO_2 nanobelts were shown in Fig. 3. The coexistence of the two titania solid phases, anatase and TiO_2(B), can be observed in the TiO_2 nanobelts obtained by calcining $H_2Ti_3O_7$ nanobelts at 600 °C for 2 h. All major diffraction peaks match the standard peaks of anatase phase well (JCPDS files no. 21-1272), while weak peaks correspond to a TiO_2(B) phase (JCPDS files no. 35-0088). TiO_2(B) phase was residual under the high temperature due to the shape limit effect of nanobelts, which made phase transformation from TiO_2(B) to anatase phase difficult [17]. When the TiO_2 nanobelts were obtained by sulfuric acid corrosion of $H_2Ti_3O_7$ nanobelts at 100 °C for 12 h, TiO_2(B) phase was transformed to anatase completely at the same calcining temperature. It should be noted that the TiO_2 nanobelts with acid corrosion exhibit higher crystallinity

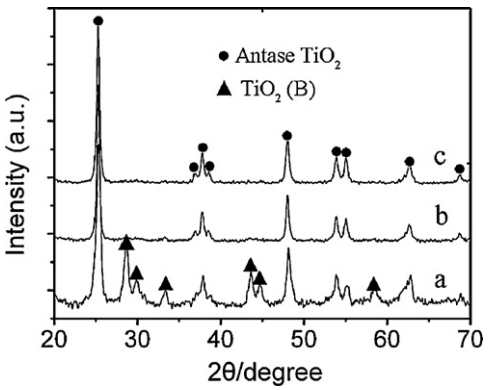

Fig. 3. XRD patterns of the as-synthesized samples: (a) TiO_2 nanobelts, (b) C–TiO_2 nanobelts and (c) Ag/C–TiO_2 nanobelts.

after the calcinations process due to the special morphology and previous phase transformation [17–19]. Here, the sulfuric acid corrosion reaction mainly proceeds through dissolving of $H_2Ti_3O_7$ and recrystallization of anatase TiO_2 on the surface of $H_2Ti_3O_7$ nanobelts. So, after the calcination process, the TiO_2 nanobelts with acid corrosion exhibit the higher crystallinity. Ag phase was not observed in XRD patterns of Ag/C–TiO_2 nanobelts due to a little of Ag, which was confirmed by TEM and EDX results.

To evaluate the photocatalytic degradation ability of TiO_2 nanobelts, C–TiO_2 nanobelts, and Ag/C–TiO_2 nanobelts, we examined the decomposition of MO in water under UV light irradiation as a function of time (Fig. 4A). For comparison, the decomposition over P25 was carried out under the same experimental conditions. The suspension was stirred in dark for 60 min to obtain the saturated adsorption of MO before illumination. However, the MO adsorption quantities of the different photocatalysts were negligible, expect for P25 with an absorption rate of 2.3%. As

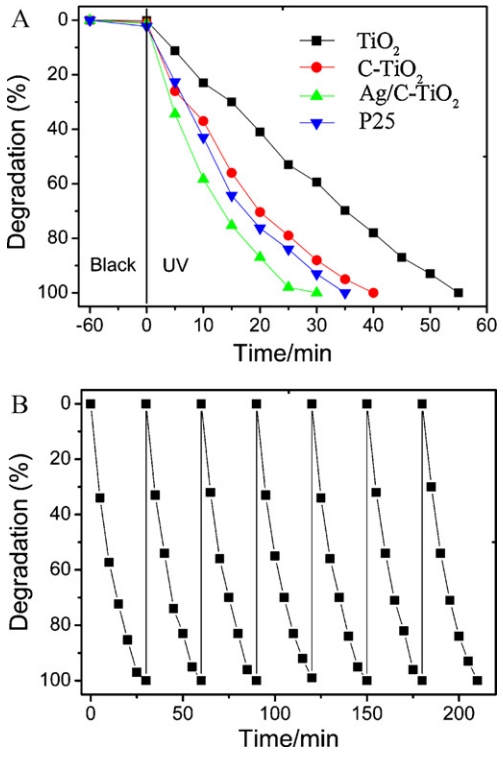

Fig. 4. (A) UV light photocatalytic degradation of MO solution in the presence of TiO_2 nanobelts, C–TiO_2 nanobelts, Ag/C–TiO_2 nanobelts and P25; (B) the photocatalytic stability of Ag/C–TiO_2 nanobelts.

shown in Fig. 4A, TiO_2 nanobelts have a low photocatalytic activity under UV-light irradiation, and the degradation rate reaches 100% in 55 min. TiO_2 nanobelts with acid corrosion have a higher photocatalytic activity, and 20 mL MO aqueous solution was completely degraded in 40 min. The enhancement of photocatalytic activity was mainly due to the rough surface with bigger specific surface area, which increases from 20.78 m^2/g of TiO_2 nanobelts to 29.13 m^2/g of C–TiO_2 nanobelts. For Ag/C–TiO_2 heterostructure photocatalyst, the complete degradation of 20 mL MO aqueous solution only needs 30 min, which was higher than that of P25. The Schottky barrier between TiO_2 and AgNPs induced the photoproduced electrons of TiO_2 to enrich on the AgNPs, which inhibited the recombination of electron and hole [20]. In order to evaluate the exact photocatalytic activity of the different photocatalysts, the parameter K was introduced here.

$$K = m_1/m_2 S_2 T$$

In the K, m_1 and m_2 are the mass of the decomposed MO and the used photocatalyst, respectively. S_2 is the surface area of the used photocatalyst. T is the photocatalytic reaction time for the complete degradation of MO.

After calculation, the K values for TiO_2 nanobelts, C–TiO_2 nanobelts, and Ag/C–TiO_2 nanobelts and P25 are 0.001, 0.0011, 0.00185 and 0.00067 $min^{-1}\ m^{-2}$, respectively. The results approve that the essential activity of different photocatalysts increases in the order of P25 < TiO_2 nanobelts < C–TiO_2 nanobelts < Ag/C–TiO_2 nanobelts. So, the BET is a dominant factor for the enhanced photocatalytic activity from TiO_2 nanobelts to C–TiO_2 nanobelts, but the Schottky barrier effect is a dominant factor for the enhanced photocatalytic activity from C–TiO_2 nanobelts to Ag/C–TiO_2 nanobelts.

The photocatalytic stability of Ag/C–TiO_2 nanobelt under UV light irradiation was shown in Fig. 4B. Herein, the repeated experiments were recycled for seven times in the same photocatalytic reactions. Taking into account the a little mass loss, the photocatalytic performance in the seven cycles has a very slight decrease in the photocatalytic activity. At the same time, the catalyst should be easily separated from solution due to the one-dimension morphology. In addition, the one-dimension structure of TiO_2 can be used for fabrication of free-standing nanopapers for the continuous photocatalysis.

Three kinds of TiO_2 nanopapers were prepared with TiO_2 nanobelts, C–TiO_2 nanobelts and Ag/C–TiO_2 nanobelts by a modified papermaking process, which were shown in Fig. 5. The mechanism of nanostructure sheet formation is similar to that of papermaking from wood fibers. The surface of the TiO_2 nanobelts is covered with hydroxyl ions in the water suspension or pulp. Since hydrogen bonding can be formed between adjacent hydroxyl groups, all the nanobelts are connected with hydrogen bondings or bridge-oxygen-atoms, and three-dimensional nanostructure nanopapers are obtained. The diameter of TiO_2 nanopapers is about 10 cm, and the thickness of the paper is determined by the concentration and volume of the nanobelt suspension. The top-view and side-view morphology of different TiO_2 nanopapers were observed. Alternative permutation of TiO_2 nanobelts formed the paper structure, which has a multi-level porous network with pore sizes of 50–500 nm. On the side-view surface of TiO_2 nanopapers, the fractured surface morphology of TiO_2 nanobelts and multilayer

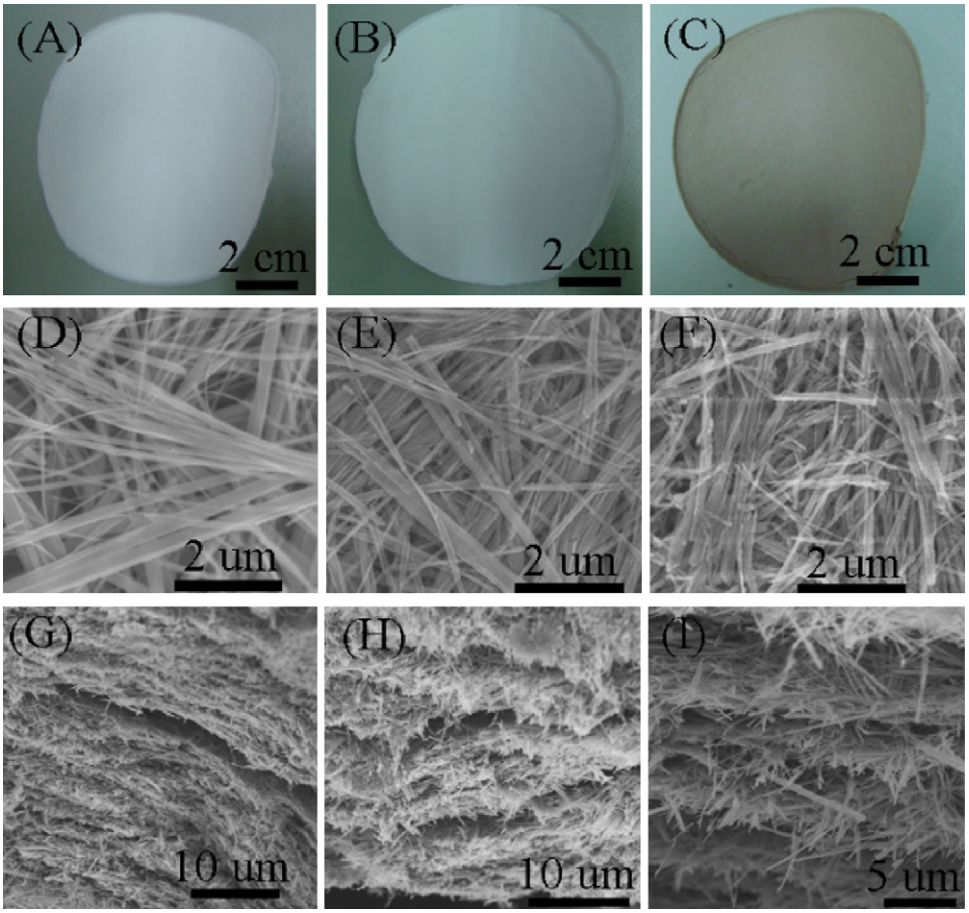

Fig. 5. Optical photographs (A–C) and SEM images (D–I) of the as-synthesized (A, D and G) TiO_2 nanopaper, (B, E and H) C–TiO_2 nanopaper and (C, F and I) Ag/C–TiO_2 nanopaper. Top view (D–F) and side view (G–I) of nanopaper.

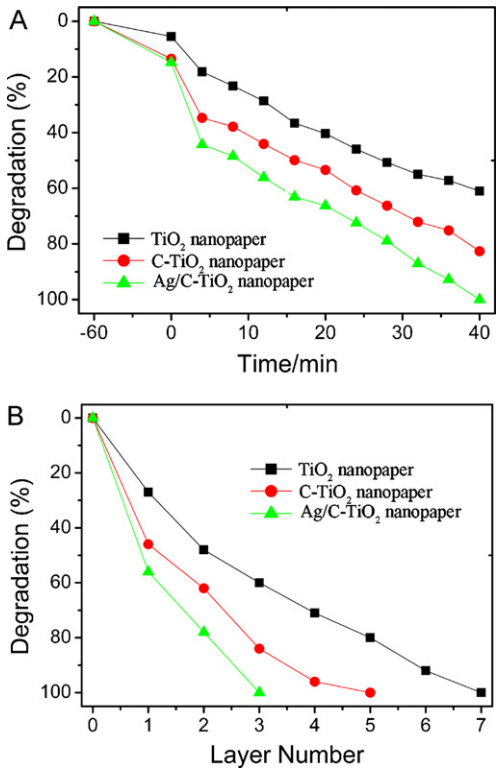

Fig. 6. Continuous-flow photocatalytic treatment of MO aqueous solution with the different TiO_2 nanopapers; (A) single layer paper with different reaction time and (B) the different layer numbers of TiO_2 papers.

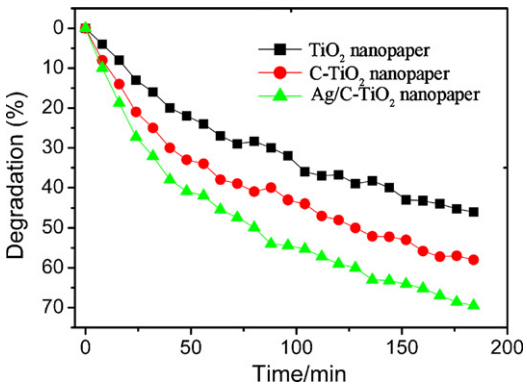

Fig. 7. Gas phase continuous-flow photocatalytic treatment of toluene gas with TiO_2, C–TiO_2 and Ag/C–TiO_2 nanopapers.

structure of TiO_2 nanopapers were observed in Fig. 5G–I, which shows that the multi-level porous structure was a 3D network. The hierarchical porous 3D network has more reaction surface, which is beneficial for the continuous-flow photocatalysis, sterilization and filtration treatment.

Continuous-flow photocatalytic treatment of MO aqueous solution with single layer TiO_2 nanopaper for different reaction time was carried out, which was shown in Fig. 6A. The simple practical reaction equipment for photocatalysis was shown in Fig. S2. The degradation rate of all samples increased with UV light irradiation time. Because of the multi-level porous structure of TiO_2 nanopapers, the strong adsorption ability for MO was observed in our experiment. As for three kinds of TiO_2 nanopapers prepared with TiO_2 nanobelts, C–TiO_2 nanobelts and Ag/C–TiO_2 nanobelts, the adsorption ratios are 5.46%, 13.5% and 14.1%, respectively. For the TiO_2 nanopaper, the decomposition rate can approach 61% after the circulation for 40 min. Under the same experimental conditions, by using C–TiO_2 and Ag/C–TiO_2 nanopapers, the decomposition ratio increases to 82.6% and 100% in 40 min, respectively. Fig. 6B shows a plot of normalized MO concentration with different layer numbers of the different TiO_2 nanopapers. To reach the degradation rate of 100%, the layer number of TiO_2, C–TiO_2 and Ag/C–TiO_2 nanopapers was 3, 5 and 7, respectively. The orange MO aqueous solution was pumped into the photocatalytic microreactor. With the UV light catalytic action between the TiO_2 nanopapers and MO aqueous solution, the clear and colorless aqueous solution was discharged from the water outlet. The hierarchical porous 3D TiO_2 nanopapers are different from TiO_2 nanoparticles loaded on substrates, which have a low photocatalytic activity due to reduction of specific surface area, reaction surface and the poor diffusive transport. Here, the hierarchical porous 3D TiO_2 nanopapers do not have non-activated substance. At the same time, the inclined surface on the inter funnels makes TiO_2 nanopapers fully receive UV light irradiation. The flowing degradation solution can remove degradation products on the surface of TiO_2 and rapidly diffuse fresh degradation solution to the photocatalyst surface, which was beneficial to the further photocatalytic reaction. Based on the reasons mentioned above, the continuous-flow photocatalysis based on TiO_2 nanopapers with a novel continuous-flow microreactor has high degradation efficiency.

Photocatalytic decomposition of toluene gas is of great significance from the viewpoint of practical application, because it is one of the typical bad odor-causing gases in indoor air [21]. The gas phase photocatalysis based on TiO_2, which was made into film or loaded on substrates, has been widely studied [22,23]. Here, the continuous photocatalytic degradation for toluene gas with five layers of TiO_2, C–TiO_2 and Ag/C–TiO_2 nanopapers were carried out, respectively, which were shown in Fig. 7. The degradation ratio for TiO_2 nanopaper was 46% in 184 min. Similarly to the reported results, at longer reaction times, the concentration of toluene was progressively reduced. The other impure peaks were not detected in gas chromatography of the degradation products, which implied that toluene gas was degraded into small molecules [24]. Furthermore, when C–TiO_2 and Ag/C–TiO_2 nanopapers were used, the degradation ratio of toluene gas achieved 58% and 69.5% after 184 min, respectively. The efficient gas photocatalytic activity for toluene was similar to that of the liquid photocatalysis, which was due to the free-standing hierarchical porous structure. Compared with the liquid photocatalysis, the gas photocatalysis needs longer reaction time. This is because that the dry toluene gas did not have water vapor, which cannot carry away the photo-induced electrons of TiO_2 photocatalyst [24]. Therefore, the photo-produced electrons and holes rapidly recombine, which induce the lower photocatalytic activity than that of the liquid phase photocatalysis.

In addition, the conventional filter paper, TiO_2, C–TiO_2 and Ag-modified C–TiO_2 nanopapers were prepared for antibacterial testing (Fig. S3). The result of antibacterial circle clearly shows the antibacterial properties of the Ag/C–TiO_2 nanopapers under dark condition, whereas no inhibition zones are observed in the control samples, including the conventional filter paper, TiO_2, and C–TiO_2 nanopapers. Therefore, it is reasonable to believe that the antibacterial property arises from AgNPs. Silver ions diffuse from the AgNPs to the bacteria suspension and agar plate. When silver ions contact *E. coli* cells, they kill the bacteria or inhibit their growth by interaction with the molecules containing S, N and P atoms in the membrane [25,26]. However, UV light has a strong bactericidal effect. With UV light irradiation, the *E. coli* strain B on the conventional filter paper, TiO_2, C–TiO_2 and Ag/C–TiO_2 nanopapers were all killed. The TiO_2 papers with a porous structure allows water or air flowing through, and retained the bacteria cells on the sheet, which were killed by Ag/TiO_2 nanobelts under dark conditions or with UV light assisted by TiO_2 nanobelts. The continuous-flow

reactor achieved by silver-modified porous TiO_2 nanostructure papers were developed, which could be used in building a disinfection device for filtering water or air [27,28].

4. Conclusions

The heterostructures, including TiO_2 nanoparticles and Ag nanoparticles, on TiO_2 nanobelts evidently enhanced the photocatalytic activity of TiO_2 nanobelts. The complete degradation of 20 mL methyl orange aqueous (MO) solution (25 mg/L) needs 55, 40 and 30 min, respectively. The nanopapers based on Ag/C–TiO_2 nanobelt heterostructures were fabricated via a modified paper-making process. A novel continuous photocatalytic reactor was designed, and MO removal rate of Ag/C–TiO_2 nanopaper was achieved to 100% in 40 min for single layer and only in 6 min for three layers. More important it is an efficient continuous photocatalysis without discontinuous time and centrifugal process. The self-supported TiO_2 nanopapers with porous structures also showed an excellent continuous photocatalytic performance for toluene gas under UV light irradiation, and the corresponding degradation rate was 69.5% in 184 min. At the same time, the Ag/C–TiO_2 nanobelt nanopapers have a good antibacterial effect. So, the multifunctional TiO_2 nanopapers modified by the heterostuctures could have potential applications in the environmental and biomaterial fields.

Acknowledgments

This research was supported by NSFC (NSFDYS: 50925205, 50872070, 60974117, grant 50990303; IRG: 51021062), the Program of Introducing Talents of Discipline to Universities in China (111 Program b06015), Independent Innovation Foundation of Shandong University (2009JC011) and Graduate Independent Innovation Foundation of Shandong University (GIIFSDU).

Appendix A. Supplementary data

Supplementary data associated with this article can be found, in the online version, at doi:10.1016/j.jhazmat.2011.09.051.

References

[1] A. Fujishima, K. Honda, Electrochemical photolysis of water at a semiconductor electrode, Nature 238 (1972) 37–38.
[2] M. Muruganandham, M. Swaminathan, Photocatalytic decolourisation and degradation of Reactive Orange 4 by TiO_2–UV process, Dyes Pigm. 68 (2006) 133–142.
[3] J. Tang, Y. Wu, E.W. McFariand, G.D. Stucky, Synthesis and photocatalytic properties of highly crystalline and ordered mesoporous TiO_2 thin films, Chem. Commun. 167 (2004) 0–1671.
[4] H.L. Fei, Y.P. Liu, Y.P. Li, P.C. Sun, Z.Z. Yuan, B.H. Li, D.T. Ding, T.H. Chen, Selective synthesis of borated meso-macroporous and mesoporous spherical TiO_2 with high photocatalytic activity, Micropor. Mesopor. Mater. 102 (2007) 318–324.
[5] J.H. Park, S. Kim, A.J. Bard, Novel carbon-doped TiO_2 nanotube arrays with high aspect ratios for efficient solar water splitting, Nano Lett. 6 (2006) 24–28.
[6] I.J. Ochuma, O.O. Osibo, R.P. Fishwick, S. Pollington, A. Wagland, J. Wood, J.M. Winterbottom, Three-phase photocatalysis using suspended titania and titania supported on a reticulated foam monolith for water purification, Catal. Today 128 (2007) 100–107.
[7] K. Hofstadler, R. Bauer, S. Novalic, G. Heisler, New reactor design for photocatalytic wastewater treatment with TiO_2 immobilized on fused silica glass fibers: photomineralization of 4-chlorophenol, Environ. Sci. Technol. 28 (1994) 670–674.
[8] E. Portjanskaja, M. Krichevskaya, S. Preis, J. Kallas, Photocatalytic oxidation of humic substances with TiO_2-coated glass micro-spheres, Environ. Chem. Lett. 2 (2004) 123–127.
[9] B. Herbig, P. Löbmann, TiO_2 photocatalysts deposited on fiber substrates by liquid phase deposition, J. Photochem. Photobiol. A 163 (2004) 359–365.
[10] T. Kasuga, M. Hiramatsu, A. Hoson, T. Sekino, K. Niihara, Formation of titanium oxide nanotube, Langmuir 14 (1998) 3160–3163.
[11] F. Zhang, R. Jin, J. Chen, C. Shao, W. Gao, L. Li, N. Guan, High photocatalytic activity and selectivity for nitrogen in nitrate reduction on Ag/TiO_2 catalyst with fine silver clusters, J. Catal. 232 (2005) 424–431.
[12] N. Sobana, M. Muruganadhaml, M. Swaminathan, Nano-Ag particles doped TiO_2 for efficient photodegradation of direct azo dyes, J. Mol. Catal. A 258 (2006) 124–132.
[13] B.F. Xin, L.Q. Jing, Z.Y. Ren, B.Q. Wang, H.G. Fu, Effects of simultaneously doped and deposited Ag on the photocatalytic activity and surface states of TiO_2, J. Phys. Chem. B 109 (2005) 2805–2809.
[14] W.J. Dong, A. Cogbill, T.R. Zhang, S. Ghosh, Z.R. Tian, Multifunctional, catalytic nanowire membranes and the membrane-based 3D devices, J. Phys. Chem. B 110 (2006) 16819–16822.
[15] Y.M. Wang, G.J. Du, H. Liu, D. Liu, S.B. Qin, N. Wang, C.G. Hu, X.T. Tao, J. Jiao, J.Y. Wang, Z.L. Wang, Nanostructured sheets of Ti–O nanobelts for gas sensing and antibacterial applications, Adv. Funct. Mater. 18 (2008) 1–7.
[16] X.W. Zhang, J.H. Du, P. Lee, D.D. Suna, J.O. Leckie, TiO_2 nanowire membrane for concurrent filtration and photocatalytic oxidation of humic acid in water, J. Membr. Sci. 313 (2008) 44–51.
[17] W.J. Zhou, L.G. Gai, P.G. Hu, J.J. Cui, X.Y. Liu, D.Z. Wang, G.H. Li, H.D. Jiang, D. Liu, H. Liu, J.Y. Wang, Phase transformation of TiO_2 nanobelts and TiO_2(B)/anatase interface heterostructure nanobelts with enhanced photocatalytic activity, Cryst. Eng. Commun. (2011), doi:10.1039/c1ce05638g.
[18] W.J. Zhou, G.J. Du, P.G. Hu, G.H. Li, D.Z. Wang, H. Liu, J.Y. Wang, R.I. Boughton, D. Liu, H.D. Jiang, Nanoheterostructures on TiO_2 nanobelts achieved by acid hydrothermal method with enhanced photocatalytic and gas sensitive performance, J. Mater. Chem. 21 (2011) 7937–7945.
[19] H.Y. Zhu, Y. Lan, X.P. Gao, S.P. Ringer, Z.F. Zheng, D.Y. Song, J.C. Zhao, Phase transition between nanostructures of titanate and titanium dioxides via simple wet-chemical reactions, J. Am. Chem. Soc. 127 (2005) 6730–6736.
[20] M.M. Mohamed, K.S. Khairou, Preparation and characterization of nano-silver/mesoporous titania photocatalysts for herbicide degradation, Micropor. Mesopor. Mater. 142 (2011) 130–138.
[21] H. Einaga, S. Futamura, T. Ibusuki, Environmental applications of semiconductor photocatalysis, Appl. Catal. B 38 (2002) 215–225.
[22] J. Araña, A. Peña Alonso, J.M. Doña Rodríguez, J.A. Herrera Melián, O. González Díaz, J. Pérez Peña, Comparative study of MTBE photocatalytic degradation with TiO_2 and Cu–TiO_2, Appl. Catal. B. 78 (2008) 355–363.
[23] F.B. Li, X.Z. Li, C.H. Ao, M.F. Hou, S.C. Lee, Photocatalytic conversion of NO using TiO_2–NH_3 catalysts in ambient air environment, Appl. Catal. B. 54 (2004) 275–283.
[24] A.J. Maira, K.L. Yeung, J. Soria, J.M. Coronado, C. Belver, C.Y. Lee, V. Augugliaro, Gas-phase photo-oxidation of toluene using nanometer-size TiO_2 catalysts, Appl. Catal. B. 29 (2001) 327–336.
[25] I. Sondi, B. Salopek-Sondi, Silver nanoparticles as antimicrobial agent: a case study on *E. coli* as a model for Gram-negative bacteria, J. Colloid. Interface Sci. 275 (2004) 177–182.
[26] L.M. Chen, L. Zheng, Y.H. Lv, H. Liu, G.C. Wang, N. Ren, D. Liu, J.Y. Wang, R.I. Boughton, Chemical assembly of silver nanoparticles on stainless steel for antimicrobial applications, Surf. Coat. Technol. 204 (2010) 3871–3875.
[27] A. Pal, S.O. Pehkonen, L.E. Yu, M.B. Ray, Photocatalytic inactivation of airborne bacteria in a continuous-flow reactor, Ind. Eng. Chem. Res. 47 (2008) 7580–7585.
[28] R.V. Grieken, J. Marugań, C. Sordo, P. Martıńez, C. Pablos, Photocatalytic inactivation of bacteria in water using suspended and immobilized silver–TiO_2, Appl. Catal. B 93 (2009) 112–118.